A. Freund[1*], M. McDermott[2†] and M. Strikman[3‡]
[1] *Institut für Theoretische Physik, Universität Regensburg, D-93040 Regensburg, Germany*
[2] *Division of Theoretical Physics, Dept. Math. Sciences, University of Liverpool, Liverpool, L69 3BX, UK*
[3] *The Pennsylvania State University, Department of Physics, University Park, 16802 PA, USA*

We present a new model for generalized parton distributions (GPDs), based on the aligned jet model, which successfully describes the deeply virtual Compton scattering (DVCS) data from H1, ZEUS, HERMES and CLAS. We also present an easily implementable and flexible algorithm for their construction. This new model is necessary since the most popular models for GPDs, which are based on double distributions incorporating their known mathematical properties, in their current form cannot describe the DVCS data when employed in a full QCD analysis. We demonstrate explicitly why this is the case and indicate the sizes and shapes that GPDs from this type of model ought to have in order to be able to describe the DVCS data. We also highlight several non-perturbative input parameters which could be used to tune the GPDs, and the t-dependence, to the DVCS data using a fitting procedure.

PACS numbers: 11.10.Hi, 11.30.Ly, 12.38.Bx

I. INTRODUCTION

Generalized parton distributions (GPDs) have been studied extensively in recent years [1–11]. This interest was spurred by the realization that these distributions are not only the basic, non-perturbative ingredients in hard, exclusive processes such as deeply virtual Compton scattering (DVCS), or exclusive vector meson production, but that they are generalizations of the well known parton distribution functions (PDFs) from inclusive reactions. GPDs incorporate both a partonic and distributional amplitude behavior and hence contain more information about the hadronic degrees of freedom than PDFs. In fact, GPDs are true two-parton correlation functions, allowing access to the highly non-trivial parton correlations inside hadrons [12].

GPDs can be broadly characterised by the following features:

- They depend on two momentum fraction variables, a dependent variable and the *skewedness* (which is the difference between the momentum fractions of two adjacent partons in the parton ladder).
- For fixed skewedness, they are continuous functions of the dependent variable and span two distinct regions, the DGLAP region and the ERBL region, in which their evolution in scale obeys generalized versions of the DGLAP and ERBL evolution equations, respectively, and in which their behavior is qualitatively different.
- They are even functions of the skewedness variable and the singlet, non-singlet and gluon distributions are either symmetric or anti-symmetric about the center point of the ERBL region (the symmetry obeyed depends on the precise definitions used).
- The Lorentz structure of their definitions implies a polynomiality condition [2,3,11,13]: their $(N-1)$-th moments are polynomials in square of the skewedness of degree no greater than $N/2$.
- They reduce to the ordinary PDFs in the limit of zero skewedness (the 'forward limit').

All of the above features are expected to be preserved under evolution in scale.

Any suggested model of GPDs should adhere to these mathematical features. In [14] such a model, based on double distributions (DDs), was suggested for the GPD input distributions (see also [15]). In [13] it was realised that an additional term, the so-called D-term, was required in the ERBL region for the unpolarized quark singlet and gluon distributions in order to satisfy polynomiality for even N. The use of DDs augmented with a D-term has become a popular phenomenological model. Unfortunately, when this type of model for input GPDs was used in its current form to calculate deeply virtual Compton scattering at both leading (LO) and next-to-leading order (NLO), the results were not in agreement with the H1 data [16] on the DVCS photon level cross section, $\sigma(\gamma^* p \to \gamma p)$, and the HERMES and CLAS data [17] on the DVCS single spin asymmetry or charge asymmetry [18–20].

Another popular model for input GPDs, inspired by the aligned jet model (AJM) [21] and its QCD extension [22] is based on the observation that at a scale $Q^2 \sim 1-2$ GeV^2 and a wide range of x_{bj}, soft physics gives the dominant contribution to the parton densities. As a result the effect of skewedness at small x_{bj} should be rather small and hence at the input scale, it is a good approximation to set the GPDs equal to the forward PDFs

*Email address: andreas.freund@physik.uni-regensburg.de
†Email address: martinmc@amtp.liv.ac.uk
‡Email address: strikman@phys.psu.edu

at the same parton fraction, X, defined with respect to the *incoming* proton [8] (for any skewedness). This has the advantage that it automatically satisfies the requirements of polynomiality for the first two moments, however one encounters infinities in the quark singlet GPD in the middle of the ERBL region.

Another 'forward model', which may be considered to be an extreme case of a DD model, was adopted in [11] where one assumes that the GPD is equal to the forward PDF at the same parton momentum fraction, v, with respect to the average of the *incoming and outgoing* proton momentum, which implicitly contains the skewedness. This translates to an X which is shifted to lower values by an amount controlled by the skewedness. This ansatz works fine for the DGLAP region. Unfortunately in the ERBL region it also involves sampling the forward PDFs right the way down to zero in momentum fraction where they have not yet been measured (this is especially problematic for singular quark distributions). In this paper we construct an alternative, finite 'forward model' for the input GPDs, using the forward input PDFs in the DGLAP region and imposing a simple form in the ERBL region that has the correct symmetries and ensures polynomiality is respected in the first two moments (see [11] for alternative ways of dealing with this problem). As we will demonstrate this forward model reproduces the available data on DVCS reasonably well.

The structure of the paper is organized as follows. In Section II, we recapitulate the DD-based models in detail and demonstrate that their problem in describing the experimental data cannot be readily side-stepped. In Section III we construct our alternative forward model for the input GPDs, which is motivated by the AJM [21,22] and describes the data well. Section IV contains a detailed explanation of why the DD-based models in their current form cannot describe the data. As an exercise, briefly suggested in [18], we present in Section V GPDs as they should emerge in size and shape from a modified DD-model which can describe the data. In Section VI we propose a phenomenological model for the slope of the t-dependence in which the slope parameter is allowed to change with photon virtuality, $q^2 = -Q^2$. The model improves the theoretical description of the Q^2-dependence of the HERA data, relative to using a constant slope. Finally we summarize our findings in Section VII.

II. THE DOUBLE DISTRIBUTION MODEL, POLYNOMIALITY AND DVCS

In this section we review some of the known features of GPDs and how these properties are implemented in popular models. We also reiterate the problem of using the unmodified DD-based model to describe the DVCS data.

GPDs are defined by Fourier transforms of twist two operators sandwiched between unequal momentum nucleon states (p, p' are the initial and final state nucleon momenta). The essential feature of such two parton correlation functions is the presence of a finite momentum transfer, $\Delta = p - p'$, in the t-channel. Hence the partonic structure of the hadron is tested at *distinct* momentum fractions. On the light cone these matrix elements are expressed through a two dimensional spectral representation, parameterized by functions called double distributions (DDs), which depend on four variables: two plus-momentum fractions with respect to two external momenta, on the four momentum transfer squared, $t = \Delta^2$, and on the renormalization scale μ^2. The external momenta can be selected in several ways (e.g. either the 'symmetric' ($\Delta, \bar{P} = (p + p')/2$), or 'natural' ($\Delta, p$) choices). Unfortunately this freedom has led to a proliferation of definitions and nomenclature for GPDs in the literature (skewed, off-diagonal, non-diagonal, off-forward, $\cdots$) to describe essentially the same objects, which has led to considerable confusion. Hence the collective name *generalized* has been introduced in an attempt to rationalise and clarify the situation.

GPDs were originally introduced in [1]. Here we use, for convenience, Ji's *off-forward* parton distributions for quarks and gluons [2] that can be probed in hard exclusive processes, for example the unpolarised helicity-preserving distributions, $H^{q,g}(v, \xi)$, with dependent variable $v \in [-1, 1]$ and skewedness $\xi = \Delta_+/\bar{P}_+$ ($\xi = x_{bj}/(2 - x_{bj})$ for DVCS). From the Lorentz structure of their definitions one can derive polynomiality conditions on their moments:

$$M_N = \int_{-1}^{1} dv v^{N-1} [H^q(v, \xi) + H^g(v, \xi)] = \sum_{k=0}^{N/2} \xi^{2k} C_{2k,N} \,. \quad (1)$$

The quark distribution may be expressed as a sum of odd and even functions (about the point $v = 0$) which correspond to the singlet and non-singlet distributions, respectively. In Ji's definition the gluon distribution is purely odd about $v = 0$. This implies that odd moments are integrals over the non-singlet quark distribution and the even moments are integrals over the sum of the quark singlet and gluon distributions. For example, the first four moments are given by

$$M_1 = \int_0^1 dv H^{q,NS}(v,\xi) = C_{0,1}\,, \tag{2}$$

$$M_2 = \int_0^1 dv v[H^{q,S}(v,\xi) + H^g(v,\xi)] = C_{0,2} + \xi^2 C_{2,2}\,, \tag{3}$$

$$M_3 = \int_0^1 dv v^2 H^{q,NS}(v,\xi) = C_{0,3} + \xi^2 C_{2,3}\,, \tag{4}$$

$$M_4 = \int_0^1 dv v^3 [H^{q,S}(v,\xi) + H^g(v,\xi)] = C_{0,4} + \xi^2 C_{2,4} + \xi^4 C_{4,4}\,, \tag{5}$$

where M_1 and M_2 are generalizations of the number density and momentum sum rules (which implies that $C_{0,1} = 3$, for three valence quarks, and $C_{0,2} = 1$ from momentum conservation).

Symmetric DDs, $F_{DD}(x,y,t,Q^2)$, were introduced in [3] with plus momentum fractions, x, y, of the outgoing and returning partons defined as shown in the left hand plot of Fig. 1. They exist on the diamond-shaped domain shown to the right of Fig. 1. The outgoing parton lines of course only have a single plus momentum relative to any particular external momenta, so Ji's distributions are related to these DDs via a reduction integral, involving $\delta(v - x - \xi y)$, along the off-vertical lines in the diamond (the dotted line corresponds to $v = \xi$):

$$H(v,\xi) = \int_{-1}^{1} dx' \int_{-1+|x'|}^{1-|x'|} dy' \delta(x' + \xi y' - v) F_{DD}(x',y'). \tag{6}$$

The DDs are therefore more general objects than Ji's distributions, however they cannot be directly related to physical observables.

For the numerical solution of the renormalization group equations in [23] the *natural* off-diagonal PDFs, $\mathcal{F}^i(X,\zeta)$, defined by Golec-Biernat and Martin [10] were preferred. They depend on the momentum fraction $X \in [0,1]$ of the incoming proton's momentum, p, and the skewedness variable $\zeta = \Delta^+/p^+ = 2\xi/(1+\xi)$ (so that $\zeta = x_{bj}$ for DVCS). For the quark case, the relationship of the quark and anti-quark distributions, $\mathcal{F}^q(X,\zeta), \mathcal{F}^{\bar{q}}(X,\zeta)$, to Ji's single function $H^q(v,\xi)$ is shown in Fig. 2 (which reproduces Fig. 4 of [10]). More explicitly, for $v \in [-\xi, 1]$:

$$\mathcal{F}^{q,a}\left(X = \frac{v+\xi}{1+\xi}, \zeta\right) = \frac{H^{q,a}(v,\xi)}{1 - \zeta/2}\,, \tag{7}$$

and for $v \in [-1, \xi]$

$$\mathcal{F}^{\bar{q},a}\left(X = \frac{\xi - v}{1+\xi}, \zeta\right) = -\frac{H^{q,a}(v,\xi)}{1 - \zeta/2}\,. \tag{8}$$

The two distinct transformations between v and X for the quark and anti-quark cases are shown explicitly on the left hand side of Eqs.(7, 8) . There are two distinct regions: the DGLAP region, $X > \zeta$ ($|v| > \xi$), in which the GPDs obey a generalized form of the DGLAP equations for PDFs, and the ERBL region, $X < \zeta$ ($|v| < \xi$), where the GPDs obey a generalized form of the ERBL equations for distributional amplitudes. In the ERBL region, due to the fermion symmetry, $\mathcal{F}^q$ and $\mathcal{F}^{\bar{q}}$ are not independent. In fact $\mathcal{F}^q(X,\zeta) = -\mathcal{F}^{\bar{q}}(\zeta - X, \zeta)$, which leads to an anti-symmetry of the unpolarized quark singlet distributions (summed over flavor a), $\mathcal{F}^S = \Sigma_a \mathcal{F}^{q,a} + \mathcal{F}^{\bar{q},a}$, about the point $\zeta/2$ (the non-singlet and the gluon, $\mathcal{F}^g$, which is built from $vH^g_{Ji}(v,\xi)$, are symmetric about this point).

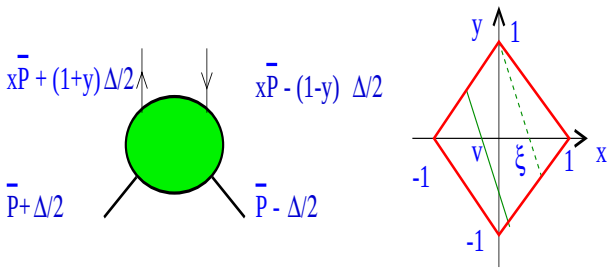

FIG. 1. Symmetric double distributions (left), indicating momentum fractions of the outgoing and returning partons, and (right) their physical domain.

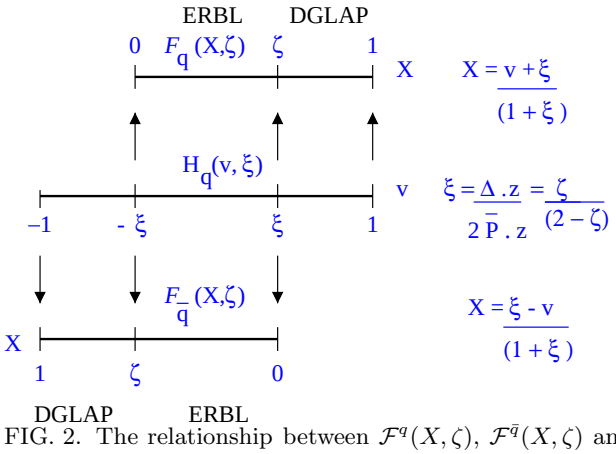

FIG. 2. The relationship between $\mathcal{F}^q(X,\zeta)$, $\mathcal{F}^{\bar{q}}(X,\zeta)$ and Ji's function $H^q(v,\xi)$ with $v \in [-1,1]$ and $X \in [0,1]$.

In [14,15] a model for $F_{DD}(x,y,t,\mu^2)$, at the input scale $\mu^2 = Q_0^2$, was introduced in which the t-dependence is assumed to be factorized, an assumption which, a priori, can only be justified for small x_{bj} and small t:

$$F^i_{DD}(x,y,\mu^2,t) = \pi^i(x,y)\, f^i(x,\mu^2)\, r^i(t) \tag{9}$$

where f^i, r^i are the standard PDF and form factor for the parton distribution of general type i. Henceforth we shall suppress the t-dependence since it is assumed to factorize. The profile functions, $\pi^i(x,y)$, are asymptotic shape functions [3] for quarks and gluons of the general form

$$\pi(x,y) = \frac{\Gamma(2b+2)}{2^{2b+1}\Gamma^2(b+1)} \frac{[(1-|x|)^2 - y^2]^b}{(1-|x|)^{2b+1}}\,, \tag{10}$$

and normalized such that

$$\int_{-1+|x|}^{1-|x|} dy\ \pi(x,y) = 1\,. \tag{11}$$

Note that π is an even function of both of its arguments [24]. The power b controls the size of the skewing effects in the input GPD. Usually $b = 1$ is chosen for the quarks, corresponding to maximum skewedness, whereas $b = 2$ is chosen for the gluons. In the limit $b \to \infty$ the forward limit of no skewedness is recovered (but only very slowly see Fig. 8 of [23] for plots of the case $b = 100$). If the assumption of a factorized t-dependence is relaxed the evolution of these distributions with μ^2 becomes much more complicated.

By design, the moments of GPDs based on double distributions are automatically polynomials in the skewedness variable, ξ. This can be seen by taking moments of both sides of Eq. (6) and by using the delta function to perform the integration over v on the right hand side:

$$\begin{aligned}
&\int_{-1}^{1} dv v^{N-1} H(v,\xi) = \\
&\int_{-1}^{1} dx \int_{-1+|x|}^{1-|x|} dy\ (x+\xi y)^{N-1}\ F_{DD}(x,y) \equiv \\
&\sum_{k=0}^{N-1} \xi^k\,(N-1k) \int_{-1}^{1} dx \int_{-1+|x|}^{1-|x|} dy\ F_{DD}(x,y)\ x^{N-1-k} y^k\,.
\end{aligned} \tag{12}$$

Performing the above integrals for a particular model for $F_{DD}(x,y)$ determines the respective coefficients in the polynomial. In order to ensure non-zero coefficients, $C_{N,N}$ of the highest power of ξ^N, for even N, one has to include an additional term, the so-called 'D-term' [13], to both the quark singlet and gluon GPD (cf. Eq. (1)). The missing (odd) powers of ξ reflect the symmetry of the matrix elements under $\xi \to -\xi$ [24].

The D-term can be computed in the chiral-quark soliton model [13,25] to be given as a truncated expansion in terms of odd Gegenbauer polynomials:

$$\begin{aligned}
&H^D(v,\xi) = \Theta(\xi - |v|)\, D\left(\frac{v}{\xi}, t=0\right)/N_F\,, \\
&D(a) = (1-a^2)\times \\
&\left[-4.0 C_1^{3/2}(a) - 1.2 C_3^{3/2}(a) - 0.4 C_5^{3/2}(a)\right]\,.
\end{aligned} \tag{13}$$

however its influence becomes negligible in the small ξ (or ζ) limit (see e.g. Fig. 7 of [23]). The restriction of the D-term to the ERBL region and the fact that it is restricted to odd functions of v/ξ guarantees that upon integration it provides the missing highest coefficient, $C_{N,N}$, for even N, without modifying the coefficients of other powers of ξ. The model of Eq. (13) gives $C_{2,2} \approx -3.2$.

Let us now reiterate [18,19] what happens in a LO or NLO QCD analysis if we pick a forward distribution 'off-the-shelf' and compare our results to available DVCS data. Our benchmark here will be the H1 data for the photon level DVCS cross section.

The triple differential DVCS cross section, on the lepton level, contains the pure Bethe-Heitler (BH) and DVCS terms, as well as an interference term, and is given in general through

$$\begin{aligned}
&\frac{d\sigma^{(3)}(ep\to e\gamma p)}{dx_{bj}dQ^2d|t|} = \int_0^{2\pi} d\phi \frac{d\sigma^{(4)}}{dx_{bj}dQ^2d|t|d\phi} = \\
&\frac{\alpha^3_{e.m.}x_{bj}y^2}{8\pi Q^4}\left(1+\frac{4M^2x_{bj}^2}{Q^2}\right)^{-1/2}\int_0^{2\pi} d\phi |\mathcal{T}|^2\,,
\end{aligned} \tag{14}$$

where

$$|\mathcal{T}|^2 = |\mathcal{T}_{\rm DVCS}|^2 \pm (\mathcal{T}^*_{\rm DVCS}\mathcal{T}_{\rm BH} + \mathcal{T}_{\rm DVCS}\mathcal{T}^*_{\rm BH}) + |\mathcal{T}_{\rm BH}|^2\,,$$

and ϕ is the relative angle between the lepton and hadron scattering planes in the special target rest frame defined in [26], Q^2 is minus the photon's virtuality, S is the total center of mass energy squared, M is the nucleon mass and $y = Q^2/x_{bj}S$ is the fraction of the scattered lepton energy carried by the photon in the target rest frame. The upper (lower) sign in front of the DVCS-BH interference term indicates a positron (electron) probe.

The photon level cross section $\sigma(\gamma^* p \to \gamma p)$ is then defined through

$$\frac{d^2\sigma^{\rm DVCS}(ep\to ep\gamma)}{dydQ^2} = \Gamma\ \sigma_{\rm DVCS}(\gamma^* p \to \gamma p) \tag{15}$$

where $\Gamma = \alpha_{e.m.}(1+(1-y)^2)/2\pi y Q^2$. Eq. (15) is obtained by integrating Eq. (14) over t, ϕ, changing variables from x_{bj} to y and then subtracting the BH contribution. Note that for small x one can completely neglect the ϕ-integrated interference term [19,20]. This then allows us to establish the formula for the photon-level cross section in terms of DVCS amplitudes as

$$\sigma_{\rm DVCS}(\gamma^* p \to \gamma p) = \frac{\alpha^2 x_{bj}^2 \pi}{Q^4 B}|\mathcal{T}_{\rm DVCS}|^2|_{t=0}, \tag{16}$$

where the slope parameter B stems from the integration over t (we have assumed a global t-dependence of the form e^{Bt}). In principle, B depends both on x_{bj} and Q^2. However, for simplicity we choose a fixed average value of 6.5 GeV^2. Note that since B has not been measured in DVCS this leads to an associated uncertainty of the normalization of the cross section (a comparison with comparable hard diffractive processes indicates that the induced uncertainty is around $30 \sim 40\%$). We will return to this point in Section VI. The details of how to compute the DVCS amplitude, $\mathcal{T}_{\rm DVCS}$, given a model for the input GPDs, can be found in detail in [19,27] and will not be repeated here.

It was shown in [19] that maximal skewing ($b = 1$) at 'conventional' input scales ($Q_0 = 1, 2$ GeV) overshoots the H1 data by a large factor. It was also demonstrated that one can describe, in LO only, the H1 data without including skewedness effects at the input scale, $Q_0 = 2$ GeV, if one neglects evolution [20]. This simplification, however, is not warranted since we know that the effects of skewed evolution are very strong in the region of $v \sim \xi$ (i.e., $X \sim \zeta$) compared to forward evolution [8,23]. Note that this region strongly influences the cross section at small x_{bj}. As we will expand on in Section IV the failure results from sampling singular forward sea distributions at extremely small x in the DD-based model. One may wonder whether one can come closer to the data by choosing a very low input scale and valence-like partons as in the GRV scenario [28], generating the rise of the PDFs/GPDs entirely through evolution. It turns out that choosing the canonical value of $b_q = 1$ and GRV98 input distributions ($Q_0 = 0.51, 0.63$ GeV in LO and NLO, respectively) the curves still overshoot the data considerably. Indeed, even if one tries to minimise the effect of the enhancement due to skewedness at the input scale, by choosing a large value of $b_q = 100$, the long lever arm in evolution still drives the prediction above the data by at least a factor of ~ 4. At this point, we have clearly reached an impasse with our DD models [29] in their current form and therefore have to consider other options.

III. THE FORWARD INPUT MODEL AND THE ALIGNED JET MODEL

In this section we revisit the logic of setting the GPDs equal to the forward PDFs by proposing an alternative forward model to that suggested in [11], with suitably-symmetrized input GPDs in the ERBL region constructed to satisfy the requirements of polynomiality for the first two moments.

In [9] DVCS was predicted to be measurable at DESY-HERA and, allowing for the freedom associated with choosing the slope parameter, B, the predictions successfully describe both the H1 data [16] and the recent ZEUS result [30,31] on the photon-level DVCS cross section. This was achieved by modelling the imaginary part of the DVCS amplitude at the input scale using the aligned jet model (AJM) [21,22]. This was then compared to the imaginary part of the DIS amplitude, calculated within the same framework, which was found to be smaller by a factor of about two. The comparison enabled the normalization of the DVCS amplitude at the input scale to be set using F_2 structure function data. The DVCS amplitude was then evolved to higher scales using LO skewed evolution in perturbative QCD.

The basic relation between the DVCS and DIS amplitudes, using the AJM, is given by

$$R = \frac{\mathrm{Im}\mathcal{T}_{\mathrm{DVCS}}}{\mathrm{Im}\mathcal{T}_{\mathrm{DIS}}} = \ln\left(1 + \frac{Q^2}{M_0^2}\right)\left(1 + \frac{M_0^2}{Q^2}\right) \simeq 1.5 - 2.5\,, \tag{17}$$

where Q^2 for the AJM is typically $1 - 3$ GeV^2 and M_0 is a hadronic scale which roughly corresponds to the lowest allowed, excited intermediate state in the s-channel. Therefore, $M_0^2 \sim 0.4 - 0.6$ GeV^2, or about m_ρ^2. The AJM neglects the contribution of quarks with large transverse momenta in the quark loop attached to the photons. It is easy to see that this contribution is more symmetric hence the AJM may somewhat overestimate the effect of skewedness. Eq. (17) can be generalized to demonstrate how the forward limit $\mathrm{Im}\mathcal{T}_{\mathrm{DVCS}} = \mathrm{Im}\mathcal{T}_{\mathrm{DIS}}$ is achieved, i.e., how the skewedness effect is reduced by giving the outgoing photon a spacelike virtuality, $q'^2 = -Q'^2$:

$$R = \frac{\mathrm{Im}\mathcal{T}_{\mathrm{DVCS}}}{\mathrm{Im}\mathcal{T}_{\mathrm{DIS}}} = \ln\left(\frac{1 + \frac{Q^2}{M_0^2}}{1 + \frac{Q'^2}{M_0^2}}\right)\frac{1 + \frac{M_0^2}{Q^2}}{1 - \frac{Q'^2}{Q^2}}\,. \tag{18}$$

This procedure allows one to derive a very important relation between the relative momentum fractions of the outgoing and returning partons, X and $-(X - \zeta)$ of the quark singlet GPD, and the virtualities of the incoming and outgoing photons

$$\lambda = \frac{X - \zeta}{X} = \frac{Q'^2}{Q^2}\,. \tag{19}$$

We illustrate this point in Fig. 3 by plotting R as a function of λ for several values of Q^2 and two values of M_0^2 to demonstrate the relative insensitivity of R (within $20 \sim 30\%$) to M_0.

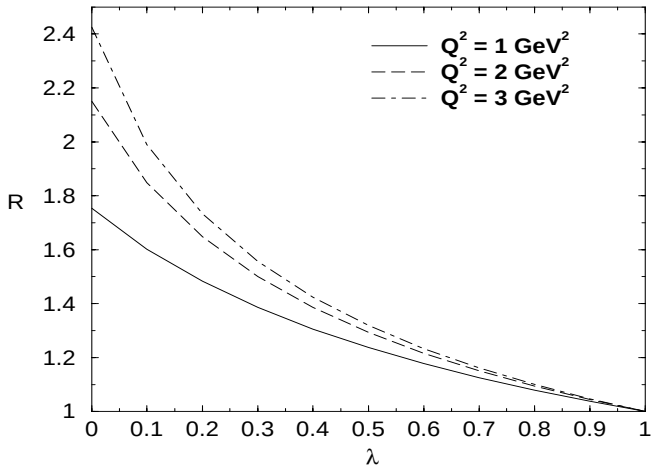

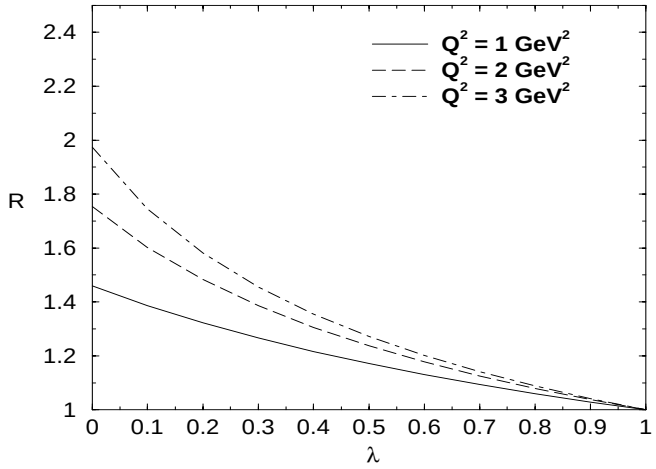

FIG. 3. The ratio R as a function of $\lambda = Q'^2/Q^2$ for several value of Q^2 and two values of $M_0^2 = 0.4$ GeV^2 (upper plot) and 0.8 GeV^2 (lower plot).

The plot shows that as X increases relative to ζ in the DGLAP region the ratio drops rapidly to its forward limit. For example, at $\lambda = 1/2$, i.e., $X = 2\zeta$, the curves are very flat and there is only a modest enhancement of $20 \sim 40\%$. One also encounters this behavior in the DD model if one investigates the ratio of the GPD to the PDF in the DGLAP region. It would therefore be advantageous to be able to directly relate R to a ratio of GPD to PDF. Trusting that perturbative QCD is applicable at the AJM input scale one can, in LO at least where the coefficient function is trivial, directly translate the ratio in amplitudes for a particular λ into a ratio of GPD to PDF:

$$R(\lambda) = \frac{\mathrm{Im}\mathcal{T}_{\mathrm{DVCS}}}{\mathrm{Im}\mathcal{T}_{\mathrm{DIS}}} = \frac{H^S(v = \xi\frac{1+\lambda}{1-\lambda}, \xi)}{q^S(X)}\,, \\ = \frac{\mathcal{F}^S\left(X = \zeta/(1-\lambda), \zeta\right)}{(1-\zeta/2)q^S(X)}\,, \qquad (20)$$

i.e.,

$$\mathcal{F}^S\left(\zeta/(1-\lambda), \zeta\right) = (1-\zeta/2)\; R(\lambda)\; q^S(X)\,. \qquad (21)$$

There are several comments in order at this point: λ is now bounded from above through $\lambda \leq 1 - \zeta$. This implies that the relationship between the ratios in Eq. (21) is only strictly true for $\lambda = 0$ (i.e., for DVCS for which $Q'^2 = 0$). The case $\lambda \neq 0$ should be viewed as follows: for $Q^2 \sim 2$ GeV^2, there is still the possibility of having more than one rung in the partonic ladder. Probing the uppermost rung with a virtuality Q^2 reveals the distribution in momentum fractions, in this case $X = \zeta$ i.e., $X - \zeta = 0$ corresponding to $\lambda = 0$. The next rung and its distribution in momentum fractions can be accessed by 'emitting' a photon with space-like virtuality (i.e., $Q'^2 > 0$). As Q'^2 increases and one goes further down the ladder to where $X \gg \zeta$, one approaches the forward limit. If one keeps the interpretation of the s-channel cut as being equal to the imaginary part of the 'scattering' amplitude for $Q'^2 \neq 0$, which, in LO, is directly proportional to GPD/PDF at $X \neq \zeta$ rather than at $X = \zeta$, then the ratio R is a direct measure of quark singlet GPD to the quark singlet PDF for $X \neq \zeta$.

If one chooses the forward model ansatz where the GPD equals the PDF at v (see e.g. [11]):

$$H^S(v, \xi) = q^S(v) \equiv q^S\left(\frac{X - \zeta/2}{1 - \zeta/2}\right)\,, \qquad (22)$$

which corresponds to the $b \to \infty$ limit of the DD model, one obtains a ratio of GPD to PDF at $X = \zeta$ of $\simeq 2$ for the quark singlet, in agreement with the AJM prediction. Hence for our forward model in the DGLAP region we choose the ansatz of Eq. (22) for the quark singlet and also the non-singlet (i.e., the valence) and the gluon. The ratios of GPD to PDF at the input scale for MRST01 quark singlet and gluon distributions [32] at LO and NLO are shown in Fig. 4. For a function which falls as x decreases, such as the valence quark at small x or the MRST gluon at LO, this ansatz leads to a suppression of the point $X = \zeta$ relative to the forward case (see the lower, dotted line in Fig. 4). Note that in NLO the MRST gluon actually goes negative at small x, so a ratio of GPD/PDF > 1 close to $X = \zeta$ in this case leads to a suppression of the DVCS cross section from the gluon contribution, relative to using PDFs. However, the DVCS cross section is rather insensitive to the behaviour of this ratio close to $X = \zeta$ for the gluon, since it only enters in NLO, and is completely insensitive to it for the non-singlet quark case since this distribution only enters into the evolution.

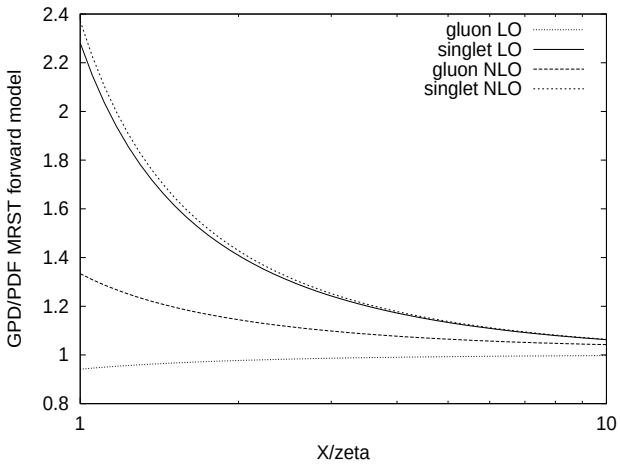

FIG. 4. The ratio GPD to PDF at $\zeta = 0.0001$ for the quark singlet and gluon, using MRST01 distributions in LO and NLO, at the input scale $Q_0 = 1$ GeV. This ratio is weakly dependent on ζ, for small ζ.

The above reasoning indicates that the physics of the AJM model provides a guide for modelling input GPDs in the DGLAP region. However it does not dictate what to do in the ERBL region, which does not have a for-

ward analog. Naturally the GPDs should be continuous through the point $X = \zeta$ and should have the correct symmetries around the midpoint of the ERBL region. They are also required to satisfy the requirements of polynomiality. At this point we choose to model the ERBL region with these natural features in mind. We demand that the resultant GPDs reproduce $M_1 \approx 3$ and $M_2 \approx 1$ (with the D-term set to zero to remove the quadratic piece in Eq. (3)). This reasoning suggests the following simple analytical form for the ERBL region ($X < \zeta$):

$$\mathcal{F}^{g,NS}(X,\zeta) = \mathcal{F}^{g,NS}(\zeta)\left[1 + A^{g,NS}(\zeta)C^{g,NS}(X,\zeta)\right] ,$$
$$\mathcal{F}^{S}(X,\zeta) = \mathcal{F}^{S}(\zeta)\left(\frac{X-\zeta/2}{\zeta/2}\right)\left[1 + A^{S}(\zeta)C^{S}(X,\zeta)\right] , \quad (23)$$

where the functions

$$C^{g,NS}(X,\zeta) = \frac{3}{2}\frac{2-\zeta}{\zeta}\left(1 - \left(\frac{X-\zeta/2}{\zeta/2}\right)^2\right) ,$$
$$C^{S}(X,\zeta) = \frac{15}{2}\left(\frac{2-\zeta}{\zeta}\right)^2\left(1 - \left(\frac{X-\zeta/2}{\zeta/2}\right)^2\right) , \quad (24)$$

vanish at $X = \zeta$ to guarantee continuity of the GPDs. The $A^i(\zeta)$ are then calculated for each ζ by demanding that the first two moments [33] of the GPDs are explicitly satisfied (remembering to include the D-term in the ERBL region which only provides the quadratic term in ξ in Eq. (2)). For the second moment what we do in practice is to set the D-term to zero and demand that for each flavour the whole integral over the GPD is equal to the whole integral over the forward PDF for the input distribution concerned (due to the inherent small errors on the PDFs, the sum of such integrals will be close to, but not precisely equal to, unity).

At small x_{bj}, which is our interest here, higher moments ($N \geq 3$) become completely irrelevant and they will be swamped by the numerical noise (which is however at most between $0.1-0.3\%$). It would be straightforward to extend this algorithm to satisfy polynomiality to arbitrary accuracy by writing the $A^i(\zeta)$ explicitly as a polynomial in ζ where the first few coefficients are set by the first two moments and the other coefficients are then randomly chosen since nothing is known about them. The above algorithm is extremely flexible both in its implementation and adaption to either other forward PDFs or other functional forms in the ERBL region. Therefore it can be easily incorporated into a fitting procedure.

In Fig. 5 we show the shape of the resulting input GPDs for two characteristic values of $\zeta = 0.001, 0.1$. The upper plot in this figure explicitly shows the antisymmetry of the singlet GPD and the symmetry of the gluon GPD about the point $X = \zeta/2$.

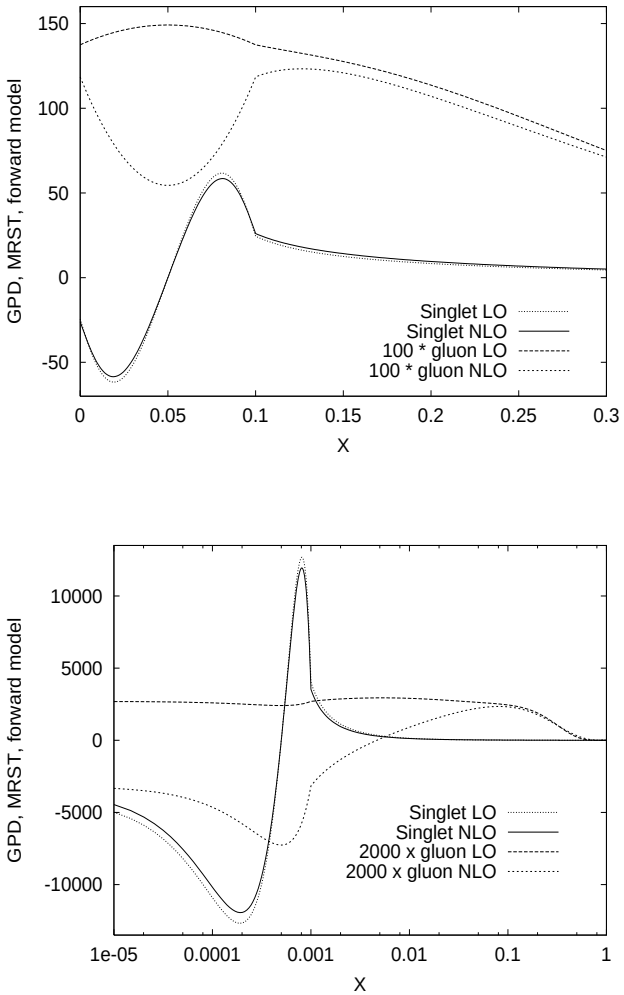

FIG. 5. The quark singlet and gluon GPDs in LO and NLO, using MRST01 input PDFs, at the input scale $Q_0 = 1$ GeV for $\zeta = 0.1$ (upper plot) and $\zeta = 0.001$ (lower plot), values typical of HERA and HERMES kinematics, respectively.

The photon level cross section results from this model, using MRST01 [32] and CTEQ6 [34] input distributions at LO and NLO, are compared in Figs. 6,7 to the H1 [16] and ZEUS [31] data at their average kinematic points, respectively. In these curves we chose to use an x and Q^2-independent slope parameter of $B = 6.5$ GeV^{-2}, but realistically there is a $30-40\%$ uncertainty associated with the value of this unknown parameter. The figures illustrate that within the framework of the forward input model for GPDs the DVCS cross section remains rather sensitive to the choice of input PDF and to the accuracy with which the calculation is performed (i.e., LO or NLO). It is important to note that the preliminary ZEUS data lies systematically above the H1 data (see Fig. 11 of [31]). Overall NLO seems to be doing better than LO, particularly on the slope of the energy dependence. It is fair to say that all of the theory curves appear to have a Q^2-dependence that is too steep to describe all of the

data. We will return to this point in Section VI.

The difference between the MRST and CTEQ curves at LO and NLO reflects the relative size of the quark singlet and gluon distributions for each set. It is possible that more precise data on DVCS may eventually allow a discrimination between various input scenarios using NLO QCD. For this to be realistic one would first need to pin down the uncertainty associated with the slope by explicitly measuring the t-dependence.

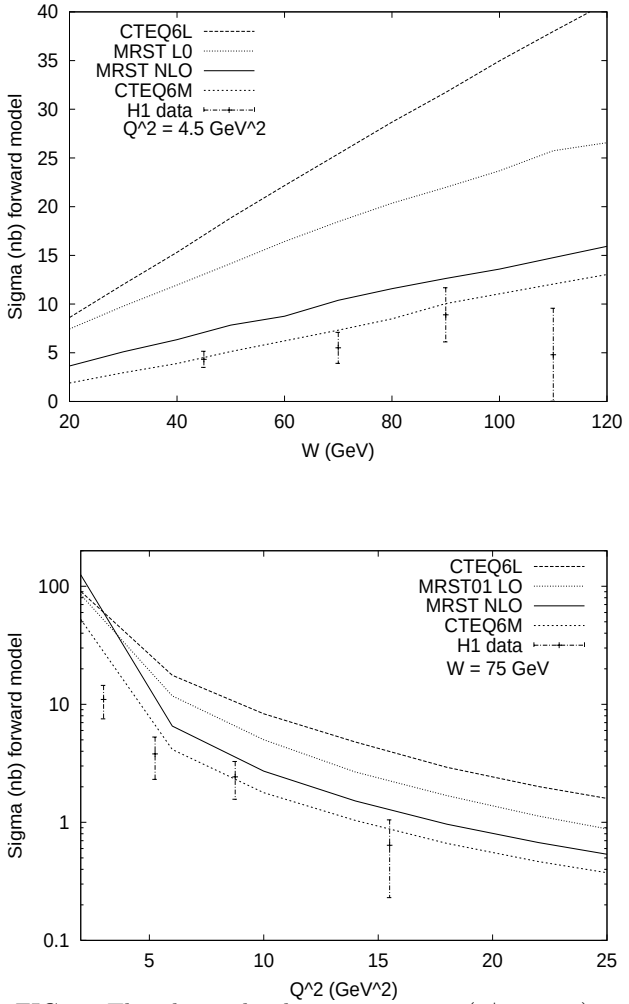

FIG. 6. The photon level cross section, $\sigma(\gamma^* p \to \gamma p)$, calculated using the forward model ansatz for input GPDs, in the average kinematics of the H1 data: as a function of W at fixed $Q^2 = 4.5$ GeV^2 (upper plot), and as a function of Q^2 at fixed $W = 75$ GeV (lower plot). A constant slope parameter of $B = 6.5$ GeV^{-2} was used.

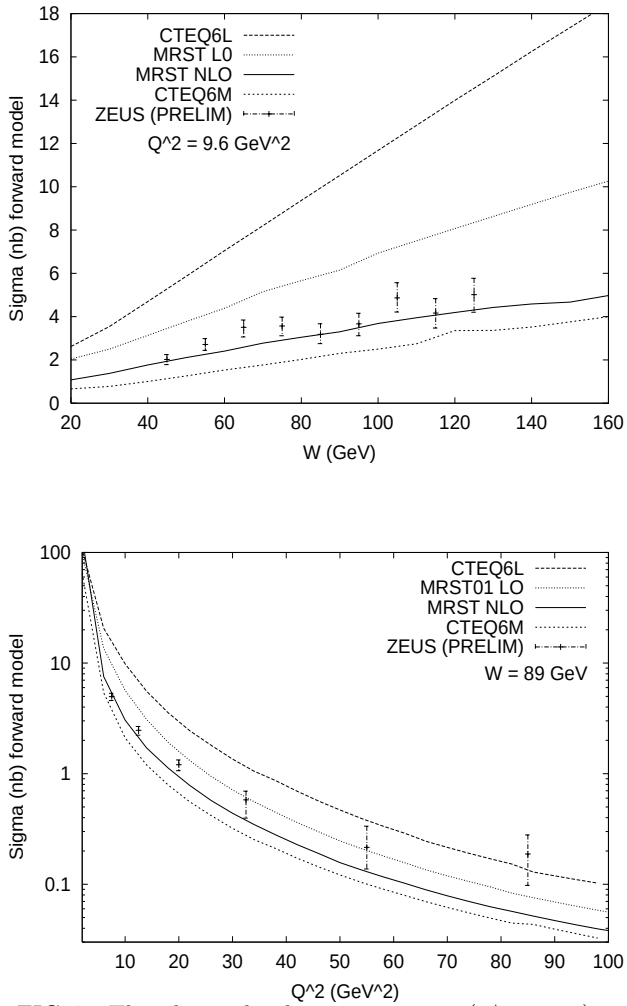

FIG. 7. The photon level cross section, $\sigma(\gamma^* p \to \gamma p)$, calculated using the forward model ansatz for input GPDs, in the average kinematics of the preliminary ZEUS data: as a function of W at fixed $Q^2 = 9.6$ GeV^2 (upper plot), and as a function of Q^2 at fixed $W = 89$ GeV (lower plot). A constant slope parameter of $B = 6.5$ GeV^{-2} was used.

We also investigated the effect on the cross section of increasing the input scale for skewed evolution using CTEQ input distributions, from the starting scale $Q_0 = 1.3$ GeV to $Q_0 = 2.0$ GeV. We then use the forward PDFs at the new scale in our model for the GPDs. Fig. 8 shows that the reduced lever arm for skewed evolution starting at the higher scale leads to a smaller cross section at LO and NLO, as expected, and that, in LO at least, the effect of this change is rather large. In fact the CTEQ and MRST collaborations only advocate the use of their forward PDFs above $Q^2 \approx 3 - 4$ GeV^2 (they start evolution at a lower scale $Q^2 \approx 1 - 2$ GeV^2 due to technicalities associated with a consistent implementation of charm). Hence, it is not completely clear where one should start skewed evolution, and this constitutes an additional uncertainty in the theoretical predictions.

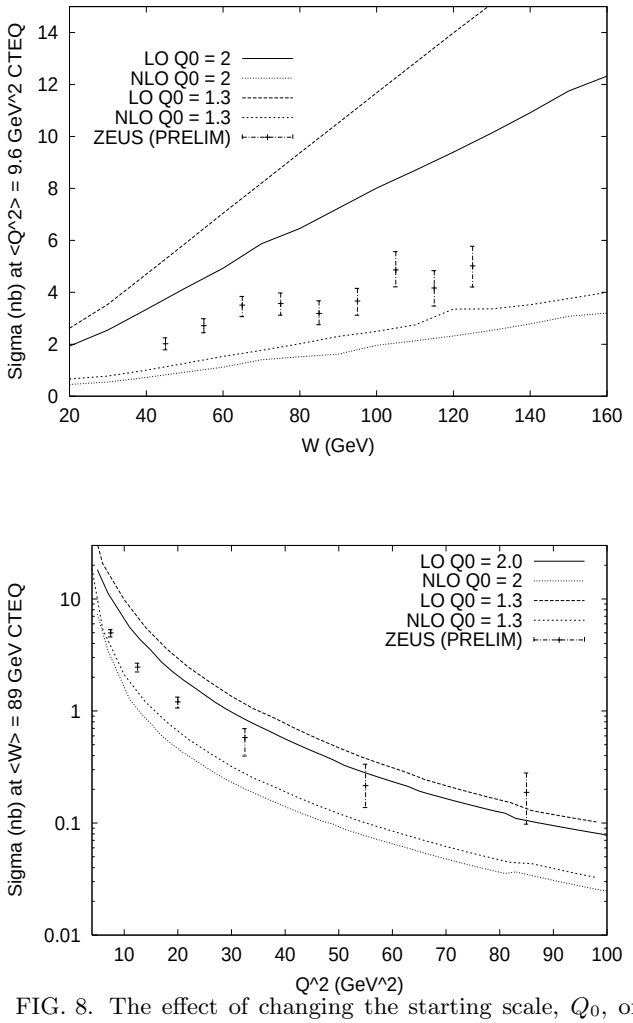

FIG. 8. The effect of changing the starting scale, Q_0, on photon level cross section $\sigma(\gamma^* p \to \gamma p)$, calculated using the forward model ansatz and CTEQ input PDFs, in the average kinematics of the preliminary ZEUS data: as a function of W at fixed $Q^2 = 9.6$ GeV^2 (upper plot), and as a function of Q^2 at fixed $W = 89$ GeV (lower plot). A constant slope parameter of $B = 6.5$ GeV^{-2} was used.

Having compared to small x_{bj} data we will now test the AJM ansatz for large x_{bj} by comparing to data on the single-spin asymmetry, SSA, (HERMES and CLAS [17]) and the charge asymmetry, CA, (HERMES only), defined by

$$SSA = \frac{2\int_0^{2\pi} d\phi\ \sin(\phi)(d\sigma^\uparrow - d\sigma^\downarrow)}{\int_0^{2\pi} d\phi\ (d\sigma^\uparrow + d\sigma^\downarrow)},$$
$$CA = \frac{2\int_0^{2\pi} d\phi\ \cos(\phi)(d\sigma^+ - d\sigma^-)}{\int_0^{2\pi} d\phi\ (d\sigma^+ + d\sigma^-)}. \qquad (25)$$

Here $d\sigma^\uparrow$, $d\sigma^\downarrow$ refer to the differential cross sections with the lepton polarised along or against its direction of motion, respectively; $d\sigma^+, d\sigma^-$ are the unpolarized differential cross sections for positrons and electrons, respectively.

Such a comparison of QCD models with the available high x_{bj} data may be viewed with some scepticism, especially in the case of CLAS which has such a low $Q^2 \sim 1-2$ GeV^2 (HERMES is only slightly better with a typical Q^2 of $\sim 2-4$ GeV^2). Firstly, it is *a priori* not clear that perturbation theory is applicable at such low Q^2 values, (in particular, higher twist corrections may be expected to become important in this region and current approximations correspond to the DVCS cross section being divergent as $Q^2 \to 0$.). Secondly, the previously neglected GPDs $\tilde{H}, E$ and $\tilde{E}$ become increasingly important as x increases [19,35]. In the following we will include the dominant twist-3 contributions [36], which are entirely kinematic in origin, in our calculation of the differential cross section, neglecting the sub-dominant twist-3 effects. We use the same input models for $\tilde{H}, E$ and $\tilde{E}$ as in [19]. For HERMES we perform a full LO and NLO QCD analysis, whereas for CLAS we are restricting ourselves to LO, i.e., we are testing handbag dominance with no or little evolution. Furthermore, we shall restrict ourselves to MRST01 input PDF for simplicity.

It transpires that the average kinematics of HERMES is such that H is still the leading GPD and within our model assumptions $\tilde{H}, E$ and $\tilde{E}$ could be set to zero for those values, with negligible difference to the final answer [37]. Within the above caveats, we find for average HERMES kinematics ($\langle x\rangle = 0.11, \langle Q^2\rangle = 2.56$ GeV$^2, \langle t\rangle = -0.265$ GeV^2) SSA $= -0.28$ (LO), -0.23 (NLO) compared to the quoted experimental result of SSA $= -0.21 \pm 0.08$ [38], and CA $= 0.12$ (LO), 0.09 (NLO) compared to CA $= 0.11 \pm 0.07$ [38]. For the average CLAS kinematics ($\langle x\rangle = 0.19, \langle Q^2\rangle = 1.31$ GeV$^2, \langle t\rangle = -0.19$ GeV^2) we find SSA $= 0.2$ (LO) compared to the experimental value of SSA $= 0.202 \pm 0.041$. This demonstrates that the AJM ansatz works surprisingly well [39] even at large x_{bj} giving us confidence in the AJM-based model and suggesting that a fit to the available data should be possible without tuning too many input parameters.

IV. THE PROBLEM WITH DOUBLE DISTRIBUTION MODELS

In this section we return to the double distribution (DD) based model described in Section II. We explain in detail why the sampling of the forward PDF at extremely small x in constructing the GPD leads to a problem in the quark singlet GPD.

It turns out that in a DD model in its current form it is of paramount importance to understand the large enhancement of the GPDs relative to the PDFs one encounters there. The key to this lies in establishing the regions in x in which the PDFs are sampled in the double distribution model, particularly at small x. Having defined the model for the double distribution in Eq. (9), with

its t-dependence factorized, one may then perform the y'-integration in Eq. (6) using the delta function. This modifies the limits on the x'-integration according to the region concerned: for the DGLAP region $X > \zeta$ ($v > \xi$) one has for the quark GPD

$$\mathcal{F}^{q,a}(X,\zeta) = \frac{2}{\zeta}\int_{\frac{X-\zeta}{1-\zeta}}^{X} dx' \pi^q\left(x', \frac{2}{\zeta}(X-x') + x' - 1\right) q^a(x')\,. \quad (26)$$

For the anti-quark GPD in the DGLAP region $X > \zeta$ ($v < -\xi$) one has

$$\mathcal{F}^{\bar{q},a}(X,\zeta) = \frac{2}{\zeta}\int_{-X}^{\frac{-X+\zeta}{1-\zeta}} dx' \pi^q\left(x', -\frac{2}{\zeta}(X+x') + x' + 1\right) \bar{q}^a(|x'|)\,, \quad (27)$$

changing variables from $x \to -x$ and exploiting the fact that the profile functions are even in both arguments one arrives at

$$\mathcal{F}^{\bar{q},a}(X,\zeta) = \frac{2}{\zeta}\int_{\frac{X-\zeta}{1-\zeta}}^{X} dx' \pi^q\left(x', \frac{2}{\zeta}(X-x') + x' - 1\right) \bar{q}^a(|x'|)\,, \quad (28)$$

so that the singlet and non-singlet quark distributions are given by

$$\begin{aligned}
&\mathcal{F}^S(X,\zeta) = \sum_a \mathcal{F}^{q,a} + \mathcal{F}^{\bar{q},a} \\
&\sum_a \frac{2}{\zeta}\int_{\frac{X-\zeta}{1-\zeta}}^{X} dx' \pi^q\left(x', \tilde{y}(x')\right)\ [q^a(x') + \bar{q}^a(x')]\,, \\
&\mathcal{F}^{NS,a}(X,\zeta) = \mathcal{F}^{q,a} - \mathcal{F}^{\bar{q},a} \\
&\frac{2}{\zeta}\int_{\frac{X-\zeta}{1-\zeta}}^{X} dx' \pi^q\left(x', \tilde{y}(x')\right)\ [q^a(x') - \bar{q}^a(x')]\,, \qquad (29)
\end{aligned}$$

where $\tilde{y}(x') = 2(X-x')/\zeta + x' - 1$.

In the ERBL region, $X < \zeta$ ($|v| < \xi$) integration over y leads to:

$$\begin{aligned}
&\mathcal{F}^{q,a}(X,\zeta) = \\
&\frac{2}{\zeta}\left[\int_0^X dx' \pi^q\left(x', \frac{2}{\zeta}(X-x') + x' - 1\right) q^a(x') - \right. \\
&\left.\int_{X-\zeta}^0 dx' \pi^q\left(x', \frac{2}{\zeta}(X-x') + x' - 1\right) \bar{q}^a(|x'|)\right]\,, \\
&\mathcal{F}^{\bar{q},a}(X,\zeta) = \\
&-\frac{2}{\zeta}\left[\int_0^{\zeta-X} dx' \pi^q\left(x', -\frac{2}{\zeta}(X+x') + x' + 1\right) q^a(x') - \right. \\
&\left.\int_{-X}^0 dx' \pi^q\left(x', -\frac{2}{\zeta}(X+x') + x' + 1\right) \bar{q}^a(|x'|)\right]\,. \quad (30)
\end{aligned}$$

Again, using $x \to -x$ and $\pi(|x'|, |y'|)$, one gets

$$\begin{aligned}
\mathcal{F}^{q,a}(X,\zeta) &= \frac{2}{\zeta}\Big[\int_0^X dx' \pi^q\left(x', \tilde{y}(x')\right) q^a(x') \\
&\quad - \int_0^{\zeta-X} dx' \pi^q\left(x', \tilde{y}(-x')\right) \bar{q}^a(x')\Big]\,, \\
\mathcal{F}^{\bar{q},a}(X,\zeta) &= -\frac{2}{\zeta}\Big[\int_0^{\zeta-X} dx' \pi^q\left(x', \tilde{y}(-x')\right) q^a(x') \\
&\quad - \int_0^X dx' \pi^q\left(x', \tilde{y}(x')\right) \bar{q}^a(x')\Big]\,. \qquad (31)
\end{aligned}$$

Hence, for the singlet and non-singlet combinations one has

$$\begin{aligned}
&\mathcal{F}^S(X,\zeta) = \sum_a \mathcal{F}^{q,a} + \mathcal{F}^{\bar{q},a} \\
&\sum_a \frac{2}{\zeta}\Big[\int_0^X dx' \pi^q\left(x', \tilde{y}(x')\right)\ [q^a(x') + \bar{q}^a(x')]\Big] \\
&- \int_0^{\zeta-X} dx' \pi^q\left(x', \tilde{y}(-x')\right)\ [q^a(x') + \bar{q}^a(x')]\Big]\,, \\
&\mathcal{F}^{NS,a}(X,\zeta) = \mathcal{F}^{q,a} - \mathcal{F}^{\bar{q},a} \\
&\frac{2}{\zeta}\left[\int_0^X dx' \pi^q\left(x', \tilde{y}(x')\right)\ [q^a(x') - \bar{q}^a(x')]\right. \\
&\left.+ \int_0^{\zeta-X} dx' \pi^q\left(x', \tilde{y}(-x')\right)\ [q^a(x') - \bar{q}^a(x')]\right]\,. \quad (32)
\end{aligned}$$

These expressions clearly satisfy the correct symmetries properties, i.e., $F^S(\zeta - X, \zeta) = -F^S(X,\zeta)$, $F^{NS,a}(\zeta - X, \zeta) = F^{NS,a}(X,\zeta)$ (n.b. $\tilde{y}(x') \to \tilde{y}(-x')$ when $X \to \zeta - X$). Analogously for the gluon one obtains

$$\mathcal{F}^g(X,\zeta) = \frac{2}{\zeta}\int_{\frac{X-\zeta}{1-\zeta}}^{X} dx' \pi^g\left(x', \tilde{y}(x')\right)\ x'g(x')\,, \quad (33)$$

for the DGLAP region, and

$$\begin{aligned}
\mathcal{F}^g(X,\zeta) &= \frac{2}{\zeta}\Big[\int_0^X dx' \pi^g\left(x', \tilde{y}(x')\right)\ x'g(x') \\
&\quad + \int_0^{\zeta-X} dx' \pi^g\left(x', \tilde{y}(-x')\right)\ x'g(x')\Big]\,, \quad (34)
\end{aligned}$$

for the ERBL region (which is symmetric under $X \to \zeta - X$).

Inspection of the integration limits in Eqs. (29, 32) highlights the main problem. In the limit $X \to \zeta$, as a result of the lower limits of the integrals the forward PDF is sampled closer and closer to $x' = 0$, where it has not yet been measured. This will be irrelevant providing the integrand is sufficiently non-singular in x' in this region i.e. it can happen if the profile functions, π^i, provide a strong suppression of this region, or if the PDFs themselves are sufficiently non-singular. However, we know that phenomenological quark and sometimes even gluon

input distributions are singular in the small x region. In the quark case this problem is made worse by the fact that we sample the number distribution $q(x')$ rather than the momentum distribution $x'q(x')$ (so that a non-singular momentum distribution $xq(x) \propto x^a$ for $a \in [0,1]$ will give a singular number distribution $q(x) \propto x^{a-1}$).

It turns out that for realistic quark distributions the region close is $x' = 0$ is very significantly sampled for small $\zeta = x_{bj}$. This leads to two serious problems. Firstly, the forward distributions are unknown here so one must extrapolate the 'known' analytic forms downwards in x'. Secondly, and much more importantly, it leads to a very significant enhancement of the quark singlet GPDs relative to the PDFs for $X \approx \zeta$, i.e., the region most relevant for DVCS. Though of paramount importance for DVCS, this region is but a small region of phase space where the current DD models fail.

We illustrate this using a series of three figures relating to the formation of the quark singlet GPD in the DGLAP region close to $X = \zeta$. Fig. 9 shows the integrand, $I(x') = \pi^u(x', \tilde{y})\ u^S(x')$, of Eq.(29) for the up quark singlet (multiplied by ζ) as a function of x'/ζ for two values of $\zeta = 0.1, 0.0001$ and two values of $X - \zeta = 0.1, 0.001$. Clearly as X approaches ζ the PDF is sampled at progressively smaller values of $x' \ll \zeta$, where for small ζ it is unknown. Fig. 10 shows the average value of x' sampled in this integral (divided by ζ) as a function of ζ for several values of $X - \zeta$. For very small values of $X - \zeta$ the average value of x' settles down to about $\zeta/4$, for small ζ. Finally in Fig. 11 we show, for MRST input PDFs, the ratio of the quark singlet GPD to PDF at $\zeta = 0.0001, 0.1$, for the canonical value of the power, $b_q = 1$, in Eq. (10). Note the large enhancement of the GPD at $X \approx \zeta$, particularly for small ζ in the upper plot. We emphasize that this enhancement, which leads to an overshoot of the DVCS data, is built in right at the start in the modelling of the quark singlet GPD at the input scale. One also sees that for the gluon, which uses $x'g(x')$, and $b_g = 2$, the ratio remains close to unity.

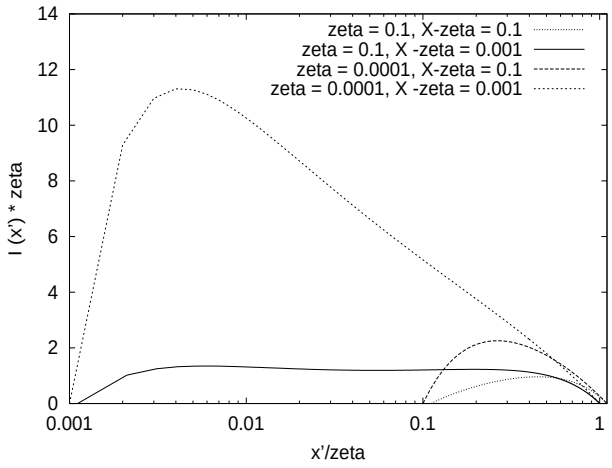

FIG. 9. The integrand of Eq.(29), illustrating how the up singlet PDF is sampled in the DGLAP region close to the boundary of the ERBL region, to produce the up singlet GPD.

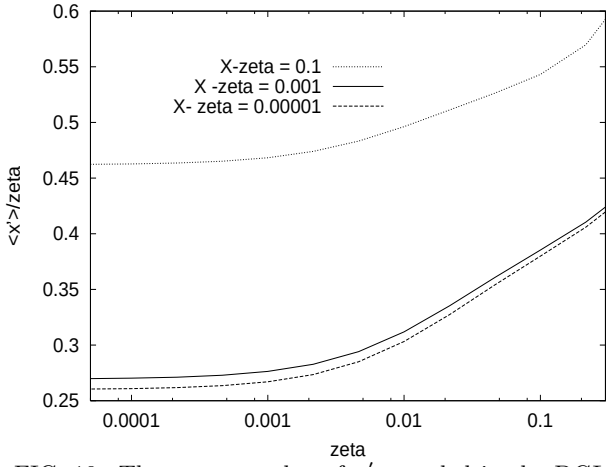

FIG. 10. The average value of x' sampled in the DGLAP region in the double distribution model, for the up singlet GPD, close to the boundary with the ERBL region as a function of the skewedness. Several values of $X - \zeta$ are shown.

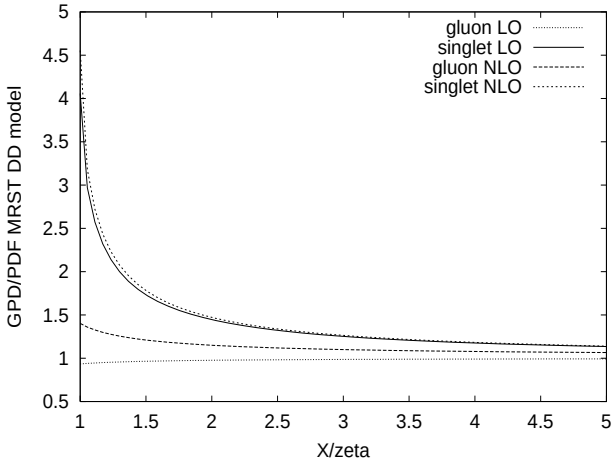

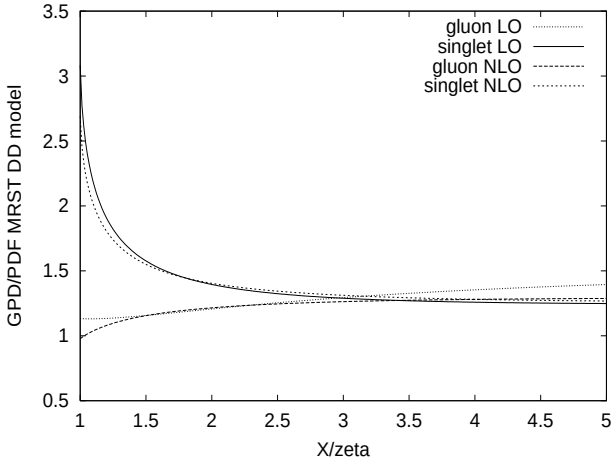

FIG. 11. The ratio GPD to PDF at $\zeta = 0.0001$ (upper plot) and $\zeta = 0.1$ (lower plot) for the quark singlet and gluon in the double distribution model, using MRST01 distributions in LO and NLO, at the input scale $Q_0 = 1$ GeV. Note the large enhancement of the quark singlet close to $X = \zeta$.

The most important enhancement effect in the valence region, $\zeta \gtrsim 0.1$, originates from the relative shift of the parton momentum fraction X to smaller values close to $X = \zeta$ (although the enhancement from small $\langle x \rangle$ is still significant). In Section III, we showed that $H(v, \xi) = (1-\zeta/2)\mathcal{F}(X, \zeta) = q(v)$ with $v = (X-\zeta/2)(1-\zeta/2)$ gives a good description of the data at both small and large x_{bj}. As stated before, this corresponds to a DD-model with $b = \infty$, i.e., with no external skewedness. However, in terms of a comparison of GPD to forward PDF, there is a residual effect of skewedness since one now has to compare $q(v)$ with $q(X)$. Since we are comparing number distributions which are more singular than momentum distributions, any shift in the momentum fraction to smaller values will lead to a quite a large enhancement of $q(v)$ relative to $q(X)$. For CTEQ6M for example the enhancement at $X = 0.1$ and $\zeta = 0.1$ is about 1.7 for the quark singlet, which increases further if more skewedness is added by decreasing b.

However, as we have demonstrated in Section III, the available data allows little room for further enhancement due to skewedness at the input scale since the LO result at least is already close to the upper bound of the experimental errors. Therefore, only the extremal "$b = \infty$" version of the current DD-model can be used to describe the data. An obvious solution to this is to modify the quark singlet profile functions in Eq.(9) in such a way as to suppress the region of very small x'. However, one must find a new functional form which achieves this without spoiling the known mathematical features of GPDs discussed above. This remains an open problem for those who wish to use the double distribution framework to model GPDs.

V. EXERCISE: WHAT SHOULD A GPD FROM A MODIFIED DOUBLE DISTRIBUTION LOOK LIKE ?

We briefly addressed the problem of sampling PDFs at extremely small x' within the double distribution model in [18] by introducing a cutoff on the integrals in Eqs. (29,32), where necessary (for the quark singlet, non-singlet and gluon). Unfortunately this procedure breaks polynomiality and therefore, formally speaking, this ansatz for input GPDs may no longer be regarded as a DD model. However, it does illustrate how the physics governing the input scale should be modelled in order to yield a GPD describing the data. As an exercise, we develop this 'model' further in this section. We will demonstrate that the breaking of polynomiality induced by the cutoff is negligible in HERA kinematics and, in fact, can easily be repaired.

We proceed in a minimal way by introducing a cutoff on the integrals in Eqs. (29,32) for the quark singlet case only, and only where necessary, i.e., when $X \approx \zeta$. Such a cutoff was briefly motivated in [18] by an analysis of the imaginary part of the DVCS amplitude. Since the cut associated with taking the imaginary part is equivalent to placing the intermediate state particle on mass shell, and this together with the requirement that the produced hadrons must a have finite mass, yields a simple kinematic argument to restrict how close X can come to ζ. At the input scale, Q_0, this gives an estimate of the size of the cutoff scale: $(Xp + q)^2 \geq m_{\rm had}^2$, i.e.,

$$X - \zeta \geq \frac{m_{\rm had}^2 \zeta}{Q_0^2} = a\zeta \,. \tag{35}$$

Choosing $m_{had}^2 = m_\rho^2 \simeq 0.5$ GeV^2 gives an estimate of $a = 0.5$ for $Q_0 = 1$ GeV (as used in e.g. [32]) Hence, for $|X-\zeta| \leq 0.5\,\zeta$, we use $x'_{min} = 0.5\,\zeta/(1-\zeta)$ for our lower cutoff in Eq. (29) and $0.5\,\zeta$ in Eq. (32). The introduction of the cutoff is only warranted for the sea quark distributions through which DVCS proceeds at small x_{bj}, it is not required for the gluon and valence distributions, since they do not directly couple to the virtual photon and thus the above argument cannot be applied to them (although, as we have argued above, the precise treatment of the region $X \approx \zeta$ in the gluon and non-singlet GPDs makes very little difference to the DVCS cross section since it is suppressed by phase space).

This adjustment in the limits of integration (rather than performing a functional change in the DD to cure the problem) breaks polynomiality and hence formally this 'model' no longer constitutes a DD-model. However, the effect of the cut-off on the final GPD will give us a hint as to what a proper DD-model should achieve in terms of size and shape of the resulting GPD.

To calculate the effect on polynomiality in introducing this cutoff on the sea distributions we set the D-term to zero and calculated M_1 and M_2 (cf. Eqs. (2,3)) which should both be constant (and approximately equal to 3 and 1 respectively). The results are plotted in Fig. 12 as functions of ξ. One can see that for small ξ i.e. $x_{bj} \leq 0.01$ modifying the sea has very little effect on M_2 ($< 2\%$). Naturally, the first moment is unchanged since we leave the valence distribution unmodified. Since we are mainly interested in small x_{bj} at this point we can easily live with this small deviation, which could be easily repaired by introducing a function in the ERBL region as in Section III which repairs polynomiality. However, given the precision of the data, worrying about a less than 2% effect is unnecessary. We note in passing that the values of the M_1 and M_2 are extremely stable with respect to the evolution of the GPDs in scale, as indeed they should

be. This is demonstrated in Fig. 13 which shows the percentage change induced in M_1 and M_2 by evolution to $Q = 5, 10$ GeV. The stability of these moments under evolution, which vary $< 0.4\%$, is another successful test of our numerical evolution package for GPDs [40].

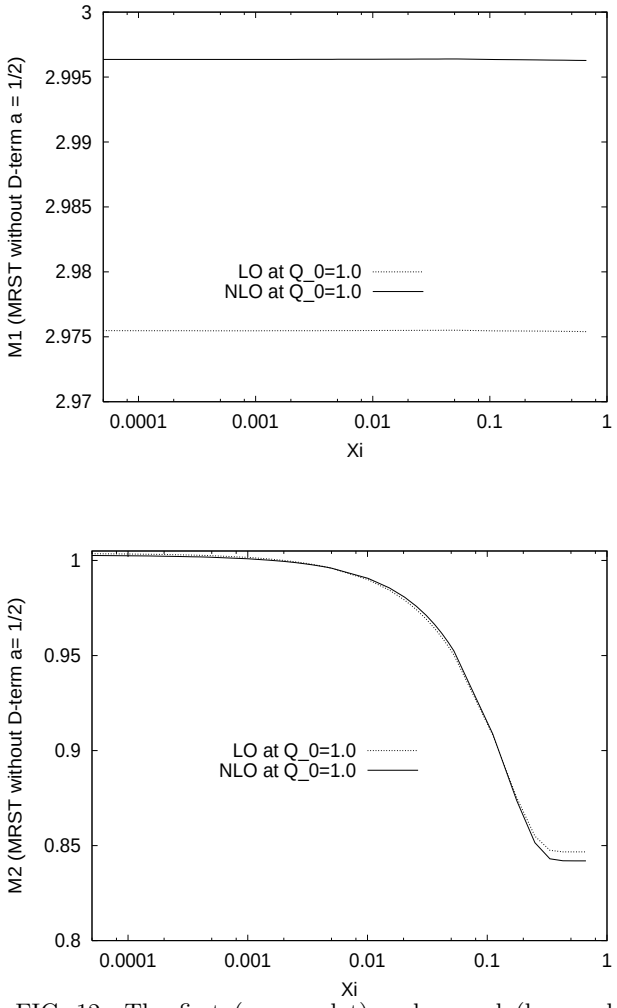

FIG. 12. The first (upper plot) and second (lower plot) moments of the input GPDs in the DD-based model. The D-term is set to zero to make any violation of polynomiality more apparent.

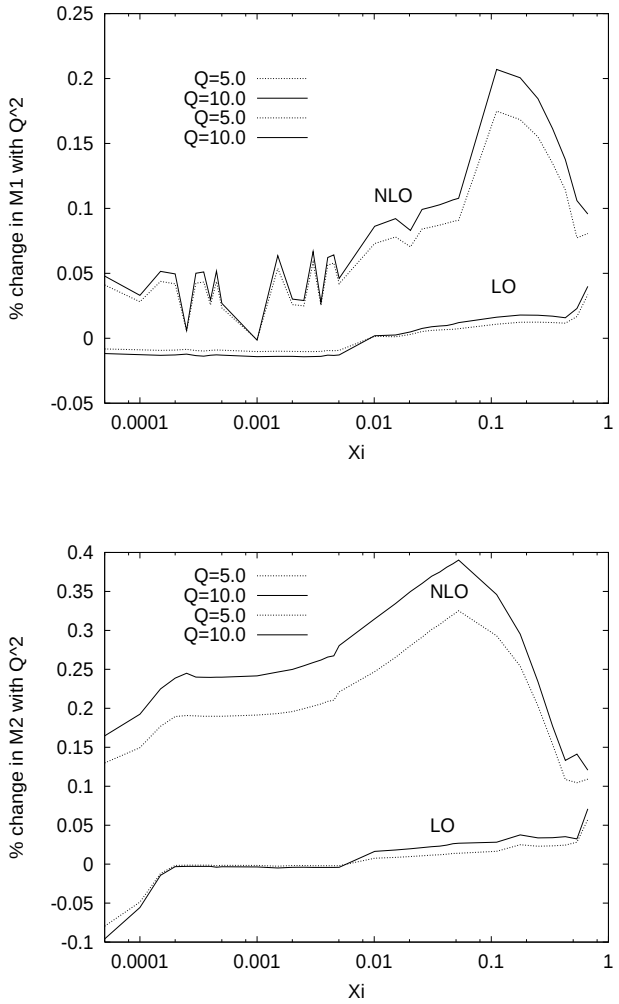

FIG. 13. The percentage deviation of the first (upper plot) and second (lower plot) moment of the GPDs evolved to two different scales.

In Fig. 14, we plot the input GPDs for our 'model' to allow a comparison with Fig. 5 of the forward ansatz. The most striking difference, in addition to the different values at $X = \zeta$, are the contrasting shapes of the quark singlet in the ERBL region (the gluon shapes are rather similar). This should lead to significant differences in the real part of the DVCS amplitudes and related observables.

The effect on the quark singlet of the cutoff is rather dramatic, the large enhancement at $X = \zeta$ that caused the problem has been significantly reduced because the quark distribution is no longer sampled at extremely small x'. In fact Fig. 15 illustrates that the quark singlet GPD is now suppressed relative to the PDF in the region $X \approx \zeta$ (cf. Fig. 4 of the forward model and Fig. 11 of the unmodified DD model).

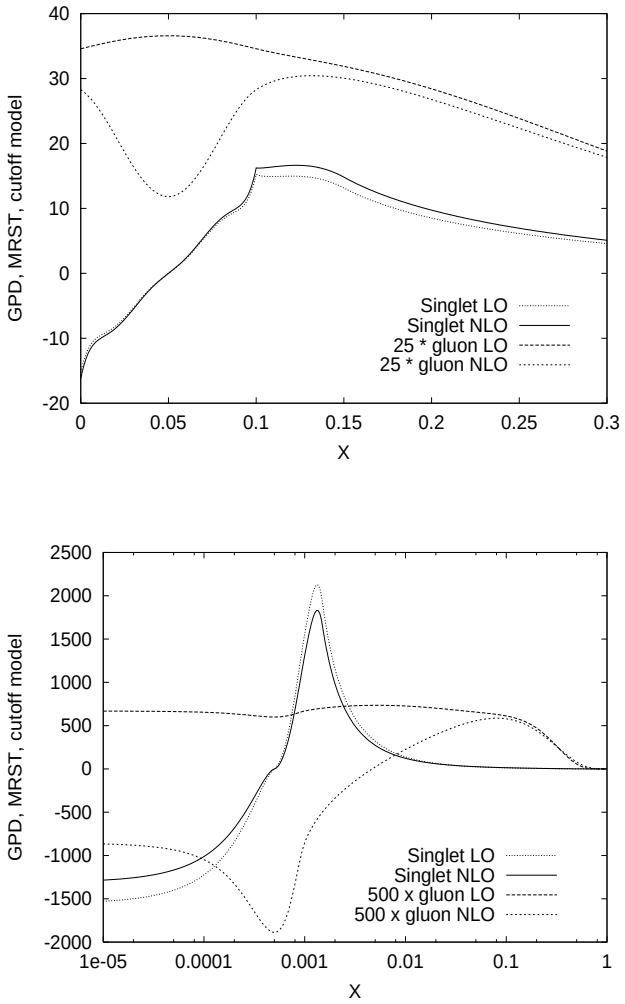

FIG. 14. The quark singlet and gluon GPDs in LO and NLO at fixed $\zeta = 0.1$ (upper plot) and $\zeta = 0.001$ (lower plot) in the DD-based cutoff model ($a = 1/2$) using MRST01 distributions in LO and NLO, at the input scale $Q_0 = 1$ GeV.

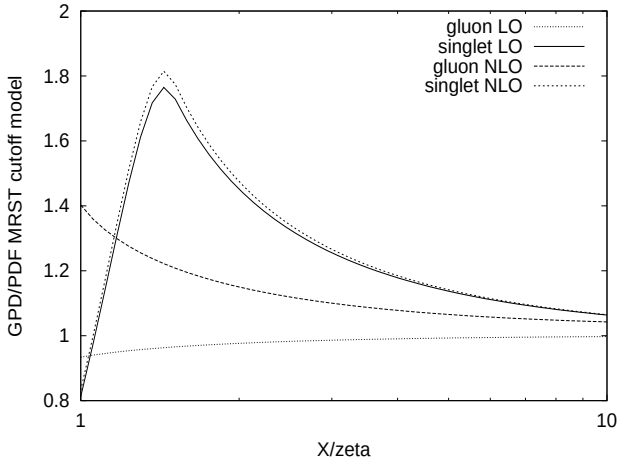

FIG. 15. The ratio of input quark singlet and gluon GPD to quark singlet and gluon PDF for MRST01 in LO and NLO at the input scale $Q_0 = 1$ GeV. Since for small ζ the above ratios hardly change at all with ζ, we only plot one curve for $\zeta = 0.0001$.

The predictions of the cutoff model for $\sigma_{\rm DVCS}(\gamma^* p \to \gamma p)$, again using $B = 6.5$ GeV^{-2}, are shown in Figs. 16,17 for CTEQ6 [34] and MRST01 [32] input PDFs at LO and NLO. With the specific value $a = 1/2$ for the cutoff parameter the cross sections come out lower than for the forward model. This is due to the reduction in the quark singlet GPD close to $X = \zeta$ (cf. Figs. 4, 15). For $a = 1/2$, MRST in NLO seems to give a good description of the H1 data but undershoots the preliminary ZEUS data. In general, the W-dependence seems to be rather well described, particularly at NLO. The same comments as in the forward model case about the B parameter and of the Q^2-dependence apply here as well.

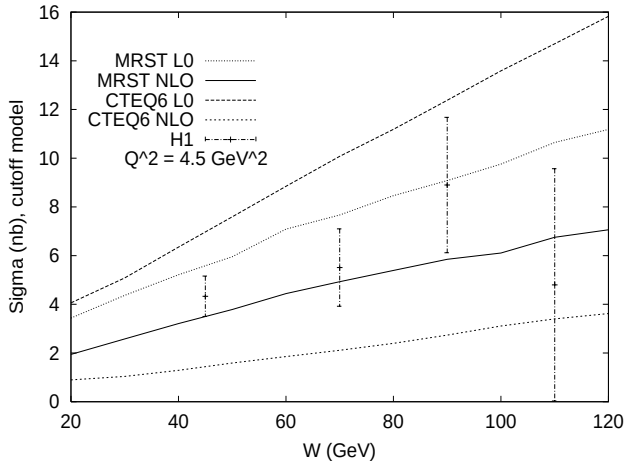

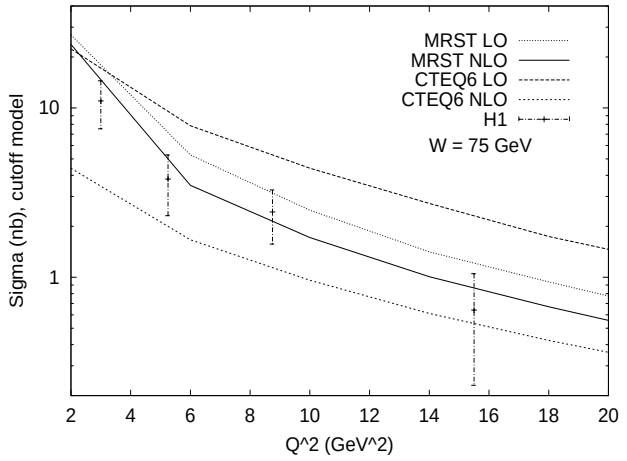

FIG. 16. The photon level cross section, $\sigma(\gamma^* p \to \gamma p)$, calculated using our 'model' for input GPDs, in the average kinematics of the H1 data: as a function of W at fixed $Q^2 = 4.5$ GeV^2 (upper plot), and as a function of Q^2 at fixed $W = 75$ GeV (lower plot). A constant slope parameter of $B = 6.5$ GeV^{-2} was used.

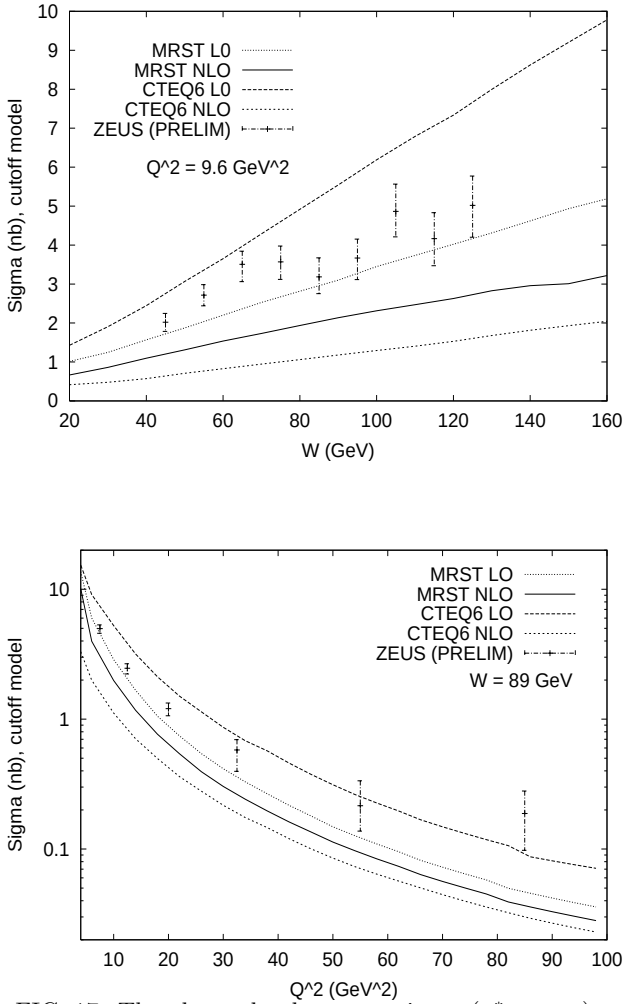

FIG. 17. The photon level cross section, $\sigma(\gamma^* p \to \gamma p)$, calculated using the cutoff DD-based model for input GPDs, in the average kinematics of the preliminary ZEUS data: as a function of W at fixed $Q^2 = 9.6$ GeV^2 (upper plot), and as a function of Q^2 at fixed $W = 89$ GeV (lower plot). A constant slope parameter of $B = 6.5$ GeV^{-2} was used.

We have also checked the results for the SSA and CA, at the average kinematical points given above, using our 'model'. In the HERMES region we found, using MRST01 input, SSA $= -0.21$ (LO), -0.17 (NLO) compared with -0.21 ± 0.08, and CA $= 0.095$ (LO), 0.08 (NLO) compared to 0.11 ± 0.07. For the CLAS region we obtained SSA $= 0.15$ (LO) compared to 0.202 ± 0.041. Compared to the AJM-inspired forward model these numbers are smaller, due to a reduced value of the GPD at $X = \zeta$, and the different treatment of the ERBL region. However, both sets of numbers fall within the current experimental errors. Lastly, it should be noted that one should not give too much weight to this model at large x_{bj} due to the strong modification originating from larger cutoffs and therefore correspondingly stronger violation of polynomiality (in the absence of a D-term the deviation of M_2 from unity reaches about 16% at the largest values of ξ, cf. Fig. 12). It is unclear whether such a strong modification of the DD at large x_{bj}, as suggested by this exercise is really necessary. However, it demonstrates that size and shape of the produced GPDs reproduce the available DVCS data fairly well. Therefore, they can be used as guidelines as to what a GPD from a properly modified DD should look like.

VI. A SIMPLE MODEL FOR THE SLOPE PARAMETER

It was pointed out in [9] that the t-slope of the DVCS cross section at small x should depend strongly on Q^2 in the transitional region from Q^2 of a few GeV^2 to large Q^2. At $Q^2 \sim 2$ GeV^2 it is natural to expect that the slope will be pretty close to that for exclusive ρ-meson production: $B \sim 8$ GeV^{-2} [41]. For large Q^2 the dominant contribution is governed by evolution trajectories which, at the resolution $Q_0^2 \sim 2$ GeV^2, originate from the gluon field. Hence we expect that in this case the slope will be given by the square of the two-gluon form factor of the nucleon at $X, X - \zeta \gg x_{bj}$. Recently [42] it was demonstrated that for $x_{bj} \geq 0.05$ this t-dependence can be approximated in a wide range of t as $1/(1 - t/m_{2g}^2)^4$ with $m_{2g}^2 \sim 1.1$ GeV^2. This corresponds to a t-slope of $B \sim 3$ GeV^{-2} for exponential fits [43]. At smaller x an increase of the slope is expected which could originate from several effects, including Gribov diffusion. Hence for the highest Q^2 point of ZEUS of about 90 GeV^2 we expect $B = 3.5 \pm 0.5$ GeV^{-2}. The recent H1 and ZEUS ρ-meson production data, for a W-range similar to the DVCS experiments, indicates that the slope of ρ-production both for σ_L and σ_T drops rather rapidly with increasing Q^2 reaching $B \sim 5$ at $Q^2 \approx 10$ GeV^2 [44].

A simple parameterization which reflects the discussed constraints for the range of $2 \leq Q^2 \leq 100$ GeV^2 is

$$B(Q^2) = B_0(1 - C \ln Q^2/Q_0^2)) \qquad (36)$$

with $B_0 = 8$ GeV^{-2}, $Q_0 = 2$ GeV^2, $C = 0.15$ being reasonable values for the various parameters. This gives $B(Q^2 = 9.6) = 6.1$ GeV^{-2} and $B(Q^2 = 4.5) = 7.0$ GeV^{-2} at the average Q^2 values of the ZEUS and H1 data, respectively (in broad agreement with our chosen constant value of $B = 6.5$ GeV^{-2}). Fig. 18 illustrates the effect of introducing this simple model on the description of the Q^2-dependence of the ZEUS data.

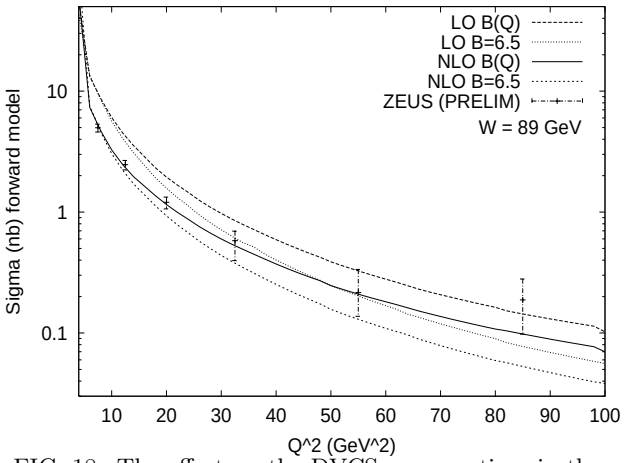

FIG. 18. The effect on the DVCS cross section, in the average kinematics of the ZEUS data, of introducing our simple Q^2-dependent model of Eq.(36) for B, the slope of the t-dependence.

This modification of the B slope gives a great improvement in comparison with the data and shows how important an experimental determination of the B slope is, since it constitutes a large theoretical uncertainty at this point.

VII. CONCLUSIONS

Using sound phenomenological guidelines such as the aligned jet model, we have constructed a model for generalised parton distributions at the input scale. Within certain theoretical uncertainties (such as the exact shape, the input scale and the functional form of B in W and Q^2) this model can be used in a NLO QCD analysis to describe the recent DVCS data from H1, ZEUS, HERMES and CLAS within their experimental errors. In constructing this model we have given a simple and flexible algorithm which can be easily incorporated into a fitting procedure.

We have also demonstrated and explained the failure of the most popular model for generalised parton distributions, the double distribution based model, to describe the available DVCS data, when rigorously applied in a LO or NLO QCD analysis in its current form. In an exercise we demonstrate what is required, in terms of size and shape, from a GPD derived from a double distribution in order to successfully describe the DVCS data. This exercise can act as a guideline for a successful modification of the original double distribution based model.

The modelling of the input GPDs is now sufficiently advanced to justify attempting to fit some of the input parameters directly to the available data. A basic analysis of the data would seem to favour a t-dependence with a slope parameter, B, that depends on Q^2. Hence, an accurate measurement of this slope is of crucial importance for further progress of the comparison of theory and experiment.

We would like to thank H. Abramowicz, C. Weiss, M. Diehl, L. Frankfurt, K. Golec-Biernat, D. Müller and A. Schäfer for helpful discussions. A.F. was supported by the DFG Emmi-Noether Program, M.M. by PPARC and M.S. by the DOE. This work is dedicated to Dina, Joanne and Patricia.

[1] D. Müller *et al.*, Fortschr. Phys. **42**, 101 (1994).
[2] X. Ji, Phys. Rev. D **55** 7114 (1997); J. Phys. G **24**, 1181 (1998).
[3] A. V. Radyushkin, Phys. Rev. D **56**, 5524 (1997).
[4] M. Diehl *et al.*, Phys. Lett. B **411**, 193 (1997).
[5] D. Müller *et al.*, Fortsch. Phys. **42**, 101 (1994).
[6] M. Vanderhaeghen, P. A. M. Guichon and M. Guidal, Phys. Rev. D **60**, 094017 (1999).
[7] J. C. Collins and A. Freund, Phys. Rev. D **59**, 074009 (1999).
[8] L. Frankfurt *et al.*, Phys. Lett. B **418**, 345 (1998), Erratum-ibid. **429**, 414 (1998); A. Freund and V. Guzey, Phys. Lett. B **462** 178 (1999).
[9] L. Frankfurt, A. Freund and M. Strikman, Phys. Rev. D **58**, 114001 (1998), Erratum-ibid. D **59**, 119901 (1999); Phys. Lett. B **460**, 417 (1999); A. Freund and M. Strikman, Phys. Rev. D **60**, 071501 (1999).
[10] K. J. Golec-Biernat and A. D. Martin, Phys. Rev. D **59**, 014029 (1999).
[11] A. G. Shuvaev *et al.*, Phys. Rev. D **60**, 014015 (1999); K. J. Golec-Biernat, A. D. Martin and M. G. Ryskin, Phys. Lett. B **456**, 232 (1999).
[12] Regular parton distributions are merely particle distributions not particle correlation functions.
[13] M. V. Polyakov and C. Weiss, Phys. Rev. D **60**, 114017 (1999).
[14] A. V. Radyushkin, Phys. Rev. D **59**, 014030 (1999).
[15] A. V. Radyushkin, Phys. Lett. B **449**, 81 (1999); I. V. Musatov and A. V. Radyushkin, Phys. Rev. D **61**, 074027 (2000).
[16] H1 Collaboration, C. Adloff *et al.*, Phys. Lett. B **517**, 47 (2001).
[17] HERMES Collaboration, A. Airapetian *et al.*, Phys. Rev. Lett. **87**, 182001 (2001); CLAS Collaboration, S. Stepanyan *et al.*, Phys. Rev. Lett. **87**, 182002 (2001);
[18] A. Freund and M. McDermott, Phys. Rev. D **65**, 091901 (2002).
[19] A. Freund and M. McDermott, Eur. Phys. J. C **23**, 651 (2002).
[20] A. V. Belitsky *et al.*, Nucl. Phys. B **629**, 323 (2002).
[21] J. D. Bjorken *et al.* Phys. Rev. D **8** 1341 (1973).
[22] L. L. Frankfurt and M. I. Strikman, Phys. Rept. **160**, 235 (1988); Nucl. Phys. B **316**, 340 (1989).
[23] A. Freund and M. McDermott, Phys. Rev. D **65**, 074008 (2002).

[24] The fact that $\pi(x,y) = \pi(x,-y)$ guarantees that odd powers of ξ are missing from the moments of $H(v,\xi)$. This is required by hermiticity and time reversal of the corresponding hadronic matrix elements.
[25] N. Kivel, M. V. Polyakov and M. Vanderhaeghen, Phys. Rev. D **63**, 114014 (2001).
[26] A. V. Belitsky *et al.*, Phys. Lett. B **510**, 117 (2001).
[27] A. Freund and M. McDermott, Phys. Rev. D **65**, 056012 (2002).
[28] M. Glück, E. Reya and A. Vogt, Eur. Phys. J. C **5**, 461 (1998).
[29] Comparison of any of the above models with data from HERMES and CLAS shows that the same problem persists also for large x_{bj}, as already pointed out in [18].
[30] ZEUS Collaboration, P. R. Saull, 'Prompt photon production and observation of deeply virtual Compton scattering', Proc. ICHEP 1999, (Tampere, Finland, July 1999), hep-ex/0003030.
[31] ZEUS Collaboration, 'Measurement of the deeply virtual Compton scattering cross section at HERA', contributed paper (abstract: 825) to ICHEP2002 (Amsterdam, July 2002).
[32] A. D. Martin *et al.*, Eur. Phys. J. C **23**, 73 (2002).
[33] The first moment counts the number of quarks in the proton and the second moment is a generalization of the momentum sum rule where the D-term generates all the deviation from unity as ξ varies.
[34] J. Pumplin *et al.*, CTEQ Collaboration, J. High Energ. Phys. **0207**, 012 (2002).
[35] A. V. Belitsky *et al.*, Nucl. Phys. B **593**, 289 (2001).
[36] A. V. Belitsky, D. Müller and A. Kirchner, Nucl. Phys. B **629**, 323 (2002).
[37] At very small t, $\tilde{E}$ becomes the large due to the pion pole it contains. However, due to other kinematical factors in front of it, the contribution from the term involving $\tilde{E}$ only becomes important close to t_{min}, which is never reached at either HERMES or CLAS.
[38] R. Shanidze, HERMES Collaboration, 'The recent HERMES results on DVCS associated asymmetries', talk at DIS 2002, (Krakow, April 2002).
[39] Unfortunately we were unable to find out what value for the slope parameter was assumed by the HERMES and CLAS experiments in producing their results for the asymmetries. In producing our values for CA and SSA we used the dipole forms for the t-dependence as presented in [19] which were taken from [35]. These forms correspond to $B \approx 6.5$ GeV^{-2}. The associated residual uncertainty is corresponding less in quantities such as SA which are sensitive to the amplitude, rather than its square.
[40] http://durpdg.dur.ac.uk/hepdata/dvcs.html
[41] ZEUS Collaboration, 'Exclusive and proton-dissociative electroproduction of ρ^0 mesons at HERA', contributed paper (abstract: 818) to ICHEP2002 (Amsterdam, July 2002).
[42] L. Frankfurt and M. Strikman, hep-ph/0205223.
[43] One needs to investigate how a change of the t-slope parameterization in the Monte Carlo used to analyse the ZEUS and H1 data would modify the extracted cross section.
[44] H1 Collaboration, 'Elastic electroproduction of ρ mesons at high Q^2 at HERA', contributed paper (abstract: 989) to ICHEP2002 (Amsterdam, July 2002).